1D-SalsaSAN: Semantic Segmentation of LiDAR Point Cloud with Self-Attention

Takahiro Suzuki, Tsubasa Hirakawa[a], Takayoshi Yamashita[b] and Hironobu Fujiyoshi[c]
Chubu University, Kasugai, Japan

Keywords: Semantic Segmenatation, Point Cloud, Self-Attention, 1D-CNN.

Abstract: Semantic segmentation on the three-dimensional (3D) point-cloud data acquired from omnidirectional light detection and ranging (LiDAR) identifies static objects, such as roads, and dynamic objects such as vehicles and pedestrians. This enables us to recognize the environment in all directions around a vehicle, which is necessary for autonomous driving. Processing such data requires a huge amount of computation. Therefore, methods have been proposed for converting 3D point-cloud data into pseudo-images and executing semantic segmentation to increase the processing speed. With these methods, a large amount of point-cloud data are lost when converting 3D point-cloud data to pseudo-images, which tends to decrease the identification accuracy of small objects such as pedestrians and traffic signs with a small number of pixels. We propose a semantic segmentation method that involves projection using Scan-Unfolding and a 1D self-attention block that is on the basis of the self-attention block. As a result of an evaluation using SemanticKITTI, we confirmed that the proposed method improves the accuracy of semantic segmentation, contributes to the improvement of small-object identification accuracy, and is sufficient regarding processing speed. We also showed that the proposed method is fast enough for real-time processing.

1 INTRODUCTION

With autonomous driving technology, it is essential to understand the environment around the vehicle. Therefore, research on autonomous driving such as object detection and semantic segmentation has attracted a great deal of attention. One such topic is semantic segmentation, which enables a detailed understanding of the environment and is classified into two methods: one using RGB (rgb, green, blue) images from in-vehicle camera images and the other using three-dimensional (3D) point-cloud data acquired from light detection and ranging (LiDAR). LiDAR can accurately acquire 3D information even at night and in bad weather conditions, which is difficult to segment using image-based methods using camera images. Because of these advantages, deep-learning-based research using omnidirectional LiDAR that acquires information in all directions has been actively conducted.

Methods using omnidirectional LiDAR can be classified as those using the acquired 3D point-cloud data without any conversion process (Ding and Feng, 2019; Liu et al., 2019; Rosu et al., 2019), converting the point-cloud data into 2D pseudo-images (Alonso et al., 2020; Simony et al., 2018; Meyer et al., 2019), and converting the point-cloud data into a voxel (Maturana and Scherer, 2015; Cheng et al., 2021; Shi et al., 2020). Methods of converting point-cloud data to pseudo-images reduces the computational cost and processing time, which are the disadvantages of using 3D point clouds, because they can execute the same processing as for images. A typical method for converting point-cloud data to pseudo-images is SalsaNext (Cortinhal et al., 2020) proposed by Tiago et al. SalsaNext is on the basis of SalsaNet (Aksoy et al., 2020), and uses the context module for global-information acquisition and a method called pixel-shuffle layer (Shi et al., 2016) for lightweight up-sampling to achieve high discrimination and real-time performance. However, the identification accuracy for small objects, such as motorcycles and signs, is low compared with that for cars and roads due to loss of data when 3D point-cloud data are converted to pseudo-images.

We propose a semantic-segmentation method called 1D salsa self-attention network (1D-SalsaSAN) by introducing a 1D self-attention

[a] https://orcid.org/0000-0003-3851-5221
[b] https://orcid.org/0000-0003-2631-9856
[c] https://orcid.org/0000-0001-7391-4725

Suzuki, T., Hirakawa, T., Yamashita, T. and Fujiyoshi, H.
1D-SalsaSAN: Semantic Segmentation of LiDAR Point Cloud with Self-Attention.
DOI: 10.5220/0011624100003417
In *Proceedings of the 18th International Joint Conference on Computer Vision, Imaging and Computer Graphics Theory and Applications (VISIGRAPP 2023) - Volume 5: VISAPP*, pages 445-452
ISBN: 978-989-758-634-7; ISSN: 2184-4321

block (1D-SAB), which is a 1D version of the SAB (Zhao et al., 2020) in SalsaNext. With 1D-SalsaSAN, self-attention of the point-cloud data of each laser ID acquired from LiDAR is calculated in order to take into account the relationship between point clouds. This enables the processing to be adapted to the characteristics of the point-cloud data acquired from LiDAR. By expressing the detailed relationship between each point cloud as weights, we can improve the identification accuracy for small objects such as motorcycles and signs, which are not identified accurately with conventional semantic-segmentation methods. In addition, a projection method called Scan-Unfolding (Triess et al., 2020) is also used to obtain pseudo-images from 3D point-cloud data. This suppresses the loss of 3D point cloud data when converting them to pseudo-images and enables feature extraction close to the original point-cloud information. The results of evaluation experiments using SemanticKITTI (Behley et al., 2019) indicates that 1D-SalsaSAN improves the accuracy of semantic segmentation by projection using Scan-Unfolding and then processing with 1D-SAB. We confirmed that it contributes to the improvement of the identification accuracy of small objects. We also showed that its processing speed is faster than that of SalsaNext.

2 RELATED WORK

Studies on omnidirectional LiDAR-based deep learning robust to nighttime and bad weather conditions, under which objects are difficult to detect with image-based methods, have been conducted, and many methods have been proposed. As mentioned above, methods using 3D point-cloud data can be categorized as those for converting 3D point-cloud data into voxels, using 3D point-cloud data without any conversion process, and converting 3D point-cloud data into 2D pseudo-images. They differ in the way they represent the point cloud. In this section, each type and the typical methods are described.

2.1 Voxel-Based Methods

Voxel-based methods first converts a 3D point-cloud data as a voxels. The voxelized point-cloud data are then input to a network consisting of 3D convolutions to obtain results. VoxelNet (Zhou and Tuzel, 2018) is a object detection method from the 3D point-cloud data divided into voxels. VoxelNet contains a feature learning network (FLN). In FLN, the 3D information is divided into equally spaced voxels, and the shape information in each voxel is obtained. The feature values of each point in the voxel are also calculated and combined with the feature values of each voxel. The feature values of each point is then used for feature extraction and output object regions.

Voxel-based methods make it easy to retain the original information of a 3D point-cloud data and smooth feature extraction by 3D convolution is possible. They also improve on the sparseness of 3D point-cloud data by grouping them by voxel, making them easier to handle for each task. However, due to the cubical representation of voxel data, this is computationally expensive and decreases the process speed.

2.2 Point-Wise Methods

With methods for using acquired 3D point-cloud-based data without any conversion process, a point cloud is directly input to a network for processing (Qi et al., 2017a; Qi et al., 2017b). The (x, y, z) coordinate information and the reflection intensity values of point clouds are input to a network.

PointNet (Qi et al., 2017a) can be applied to several tasks such as three-class classification and segmentation. It is composed of a spatial transformer network (STN), classification network, and segmentation network. First, we reduce the noise for the input point cloud in the STN. The next step is to extract the features of each point cloud from the convolution process by using the classification network. Max pooling is then used to extract the overall features and classify them. For segmentation, the overall features extracted in the classification network and the local features of each point cloud are combined and input to the segmentation network. The convolution process is executed several times again, and segmentation is executed for each point cloud. PointNet may lack detailed spatial information, thus may not be able to capture the local structure. Threfore, PointNet++ (Qi et al., 2017b) have been proposed to solve this problem, which applies the PointNet process hierarchically. It is also possible to extract pseudo-local features by inputting neighboring points that have been clustered. This solves the problems with PointNet and improves the accuracy of class classification and segmentation.

Thus, the original information of a 3D point-cloud data is retained, and accurate feature extraction is possible. These methods also eliminates the computational cost of converting to voxels, etc. However, processing 3D point-cloud data as they are requires a huge amount of storage space. The associated computational cost of processing point-cloud data is also high, which may result in a reduction in processing speed.

2.3 Pseudo-Image-Based Methods

With methods of converting a point-cloud data to pseudo-images, the coordinates of the 3D point-cloud data on a 2D pseudo-image are first calculated. Pseudo-imaging is executed by plotting each point on its coordinates. The converted pseudo-image is subjected to a 2D convolutional process similar to that for normal images and used for various tasks such as object detection and semantic segmentation. A typical method is SalsaNext (Cortinhal et al., 2020).

SalsaNext is a semantic-segmentation method that converts 3D point-cloud data acquired from omnidirectional LiDAR into pseudo-images. The problem with other such methods is that the entire network is missing context information. To solve this problem, SalsaNext introduces a context module on the basis of SalsaNet (Aksoy et al., 2020), which enables global context information to be obtained at the early stage of the network. In addition, residual expansion convolution with a residual block (He et al., 2016) is used in the encoder and decoder to obtain detailed spatial information. These interact to enable extraction of local and global features. By using dilated convolution (Lin et al., 2018) to expand the kernel size, the number of parameters for expanding the receptive field is decreased. Furthermore, the lightweight upsampling method pixel-shuffle layer (Shi et al., 2016) is used in the decoder. Pixel-shuffle layer executes upsampling by sorting the output feature map, so it has no weights, which decreases the computational cost. As described above, SalsaNext achieves high identification and real-time performance by introducing modules to increase processing speed and improve segmentation accuracy.

The advantage of this method is that the 3D point-cloud data can be used as a 2D image, which decreases computational cost and increases processing speed. The disadvantage is that the representational power of the 3D point cloud may be lost, for example, a pixel and its neighboring pixels in the converted pseudo-image are not neighboring points in the original point cloud.

2.4 Problems with Conventional Methods

The methods of converting 3D point-cloud data into voxels and using such data without any conversion process require huge computational cost in processing the acquired 3D point-cloud data, which may decrease the processing speed. Conventional methods in the 2D Images approach convert 3D point-cloud data to pseudo-images to decrease computational cost and increase the processing speed, which are the problems of two above methods. Therefore, many conventional methods using pseudo-images have real-time capability to match the driving speed of a car, which is essential for autonomous driving. However, since a large amount of data is lost when converting 3D point-cloud data to pseudo-images, it is not possible to obtain the features of small objects, e.g., motorcycles and signs with relatively small point clouds, and the identification accuracy for such objects tends to be low.

3 PROPOSED METHOD

The 3D point-cloud data acquired from omnidirectional LiDAR are dense in the horizontal direction. Due to this characteristic, the resulting pseudo-image also has more pixels in the horizontal direction and less point-cloud data is lost. Our 1D-SalsaSAN uses a 1D-SAB that focuses only on the horizontal direction to improve the identification accuracy for small objects. In this section, we describe the processing flow of 1D-SalsaSAN.

3.1 Processing Flow

Figure 1 shows the flow of 1D-SalsaSAN. It first converts the 3D point-cloud data into a pseudo-image. The vertical size of the pseudo-image is 64, which matches the LiDAR used in this study, and the horizontal size is 2048 because the horizontal irradiation interval of LiDAR is 0.175 degrees. The number of channels is 5: x, y, z, intensity, and depth. Next, the vertical coordinate of the pseudo-image is input to the 1D-SAB as the 1D-waveform data of each laser ID in LiDAR. In the 1D-SAB, relationships between point clouds are taken into account in the processing. The feature map output from 1D-SAB is then input to SalsaNext (without the context module) for convolutional processing. If the 1D-SAB is simply added as a module, the processing speed will decrease. For autonomous driving, the processing speed is as important as the identification accuracy, so the context module is removed from SalsaNext. The class probability for each pixel of the pseudo-image is then calculated using the softmax function, and each point of the original 3D point-cloud data is segmented by post-processing on the basis of the k-nearest neighbor (kNN) method.

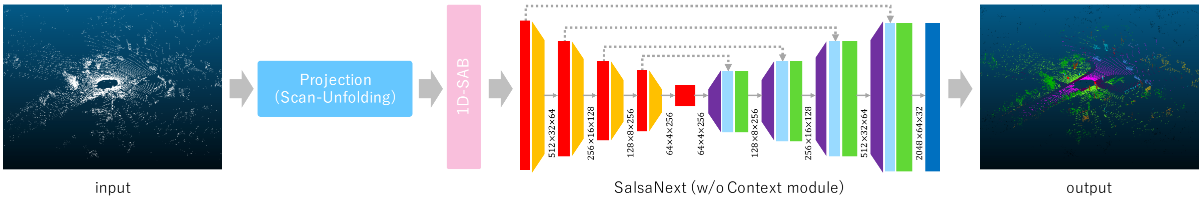

Figure 1: Overview of proposed method.

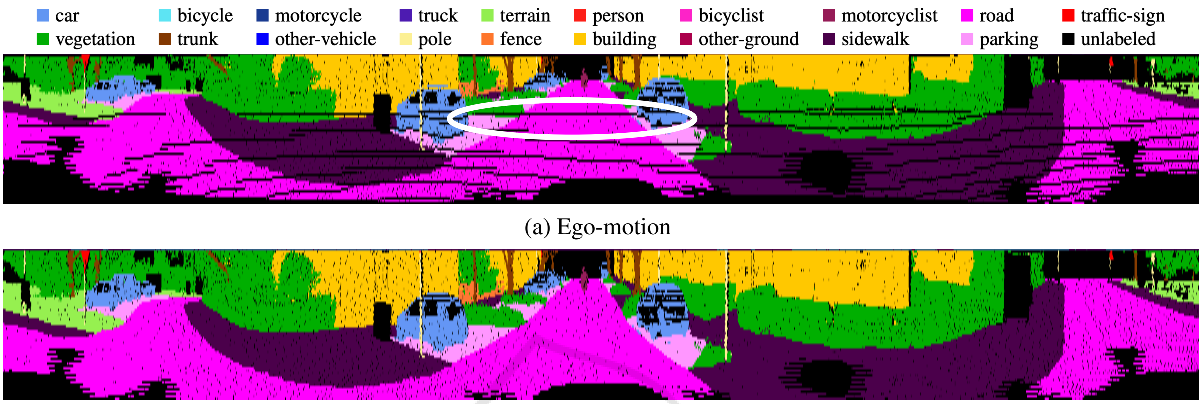

(a) Ego-motion

(b) Scan-Unforlding

Figure 2: Example of conversion of 3D point cloud data to pseudo-image.

3.2 LiDAR Point Cloud Representation

Conventional methods such as SalsaNext use Ego-motion Corrected (Milioto et al., 2019) proposed by Milioto et al. as the projection method. In contrast, 1D-SalsaSAN uses Scan-Unfolding (Triess et al., 2020) for 3D point-cloud data. Figure 2 shows an example of pseudo-images generated using Ego-motion Corrected and Scan-Unfolding. In Ego-motion Corrected (Figure 2(a)), some data are lost when 3D point-cloud data are converted to a pseudo-image (black pixels as shown in the white frame). This is due to the fact that when calculating the coordinates (u,v) on the pseudo-image for the projection of each point in 3D, different points will be on the same pseudo-image coordinates, resulting in an occlusion of the points. Scan-Unfolding executes projection in accordance with the order of the point-cloud data acquired by LiDAR. First, only the horizontal coordinate u of each point on the pseudo-image is calculated using Equation 1.

$$u = \frac{1}{2}[1 - \arctan(y,x)\pi^{-1}] \tag{1}$$

Next, the width between each neighboring point of the u coordinate is calculated, and if it is more than the threshold, the laser ID is considered to have changed and the vertical coordinate v is shifted to the bottom. Projection in this manner reduces the occlusion of points with v coordinates on the pseudo-image and suppresses the loss of point-cloud data, as shown in Figure 2(b).

3.3 1- Dimensional Self-Attention Block (1D-SAB)

We now explain the 1D-SAB. Figure 3 shows the detailed structure of 1D-SAB. The pseudo-image is considered as 1D-wave data for each laser ID and input to the 1D-SAB. Here, we denote input feature for the 1D-SAN as **h**, where the input size is $[1 \times w$ (width of the pseudo-image) $\times c$ (channels)$]$. The input data are processed one point at a time, and the self-attention of the corresponding point is calculated. When the red value in Fig. 3 is the point of interest for the process h_t, the green h_{t-1} is neighborhood 1, and the blue h_{t+1} is neighborhood 2. For each neighboring point, we apply point-wise convolution.

We input the points of interest and neighboring points into the learnable functions $\varphi(\cdot)$ and $\psi(\cdot)$. Then, the outputs of $\varphi(\cdot)$ and $\psi(\cdot)$ are used for the relational function δ, which is defined as

$$\begin{aligned} \delta(\varphi(h_t), \psi(h_{t-1})) = \varphi(h_t) - \psi(h_{t-1}), \\ \delta(\varphi(h_t), \psi(h_{t+1})) = \varphi(h_t) - \psi(h_{t+1}). \end{aligned} \tag{2}$$

The mapping function $\gamma(\cdot)$ then aligns the number of channels with the output of the first process. We then we calculate the element-wise product with the above-mentioned features by point-wise convolution.

The self-attention map (SAM) is generated by executing this process for neighboring points and summing them up. The generated SAMs are made to have the same number of channels as the input channels by point-wise convolution. The input data are added to this outputs as a skip mechanism to form the final output. By using the 1D-SAB, we can give a large weight to the important positions among the point clouds and represent the relationship between point clouds. Therefore, it is possible to obtain detailed features of a point cloud.

3.4 Loss Function

For the loss function, we use a linear combination of weighted cross-entropy loss and *Lovász-Softmax* loss (Berman et al., 2018) on the basis of the SalsaNext. The weighted cross-entropy loss is defined by

$$\begin{aligned} \mathcal{L}_{wce}(y,\hat{y}) &= -\sum_i \alpha_i p(y_i) log(p(\hat{y}_i)), \\ \alpha_i &= 1/\sqrt{f_i}\ , \end{aligned} \tag{3}$$

where y_i is the correct label, $\hat{y}_i$ is the predicted label, and f_i is the frequency (number of points) of the i^{th} class. Weighted cross-entropy is used to correct for class-specific imbalances in the dataset. Also, *Lovász-Softmax* loss is defined by

$$\begin{aligned} \mathcal{L}_{ls} &= \frac{1}{|C|}\sum_{c\in C}\overline{\Delta J_c}(m(c)), \\ m_i(c) &= \begin{cases} 1-x_i(c) & \text{if } c = y_i(c) \\ x_i(c) & \text{otherwise} \end{cases}, \end{aligned} \tag{4}$$

where $|C|$ denotes the class number, $\overline{\Delta J_c}$ defines the Lovász extension, and $x_i(x) \in [0,1]$ and $y_i(c) \in \{-1,1\}$ hold the predicted probability and ground-truth label of pixel i for class c, respectively. Finally, the total loss function can be expressed as follows: $\mathcal{L} = \mathcal{L}_{wce} + \mathcal{L}_{ls}$.

3.5 Post-Processing

Pseudo-image-based methods may not be able to correctly provide prediction results to 3D point clouds after inferring the class probabilities. Therefore, we used, post-processing on the basis of the kNN method (Milioto et al., 2019) to provide more accurate prediction results to the 3D point cloud. With this post-processing method, prediction labels are determined for each pixel of the pseudo-image on the basis of the kNN method. Next, which of the original 3D point-cloud data each pixel falls into is determined in accordance with the calculated (u,v) coordinates. The final prediction result for each pixel is then provided to the corresponding 3D point cloud. For more details, we refer the readers to a previous study (Milioto et al., 2019). Note that this post-processing is applied to the network output during inference only and has no effect on learning.

4 EXPERIMENTS

In this section, we discuss the evaluation of 1D-SalsaSAN.

4.1 Experimental Settings

We evaluated the effectiveness of 1D-SalsaSAN by comparing its accuracy and processing speed with those of conventional methods that also use pseudo-images. The conventional methods were SqueezeSeg (Wu et al., 2018), SqueezeSegV2 (Wu et al., 2019), RangeNet++ (Milioto et al., 2019), and SalsaNext (Cortinhal et al., 2020). To evaluate the effectiveness of the 1D-SAB, we assumed that Scan-Unfolding is used as the projection method for SalsaNext. For the training settings, we set the number of training epochs to 300 and batch size to 24. The optimizer was MomentumSGD, and the initial learning rate was 0.01 (decayed by 0.01 per epoch during training). We used intersection over union (IoU) between the segmentation result and the correct answer label for each point cloud as the evaluation metrics.

The overall evaluation metric is Mean-IoU (mIoU), which is the average of the IoU of each class.

4.2 Dataset

We used SemanticKITTI (Behley et al., 2019) for our evaluation. SemanticKITTI is a real-world dataset that is annotated for all point-cloud data in the KITTI dataset (Geiger et al., 2012). The dataset consists of 22 scenes and 43,000 frames. Of these, 23,201 frames from scenes 00 to scene 10 were used for training, and 20,351 frames from scenes 11 to scene 21 were used for evaluation. Among the training scenes, 4,071 frames of scene 08 were used as the validation data for training. The identification target was 19 classes.

4.3 Quantitative Results

Table 1 lists the accuracies of the conventional methods and the 1D-SalsaSAN.

Evaluating the Effectiveness of 1D-SAB. From Table 1, 1D-SalsaSAN improved in terms of mIoU by 1.1 ppt compared with SalsaNext. When comparing the accuracy of each class, the IoU of 7 among

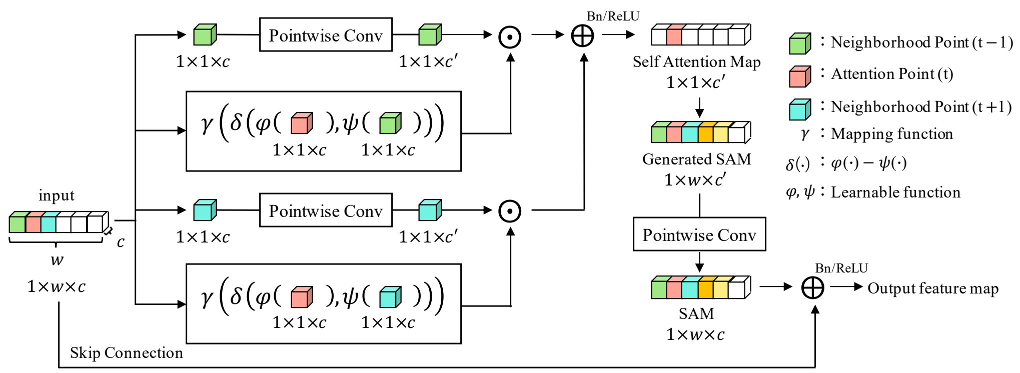

Figure 3: Detailed structure of 1D-SAB.

Table 1: Quantitative comparison on SemanticKITTI test set (sequences 11 to 21). IoU scores are given in percentage [%].

Method	car	bicycle	motorcycle	truck	othe-vehicle	person	bicyclist	motorcyclist	road	parking	sidewalk	other-ground	building	fence	vegetation	trunk	terrain	pole	traffic sign	mean-IoU
SqueezeSeg	68.3	18.1	5.1	4.1	4.8	16.5	17.3	1.2	84.9	28.4	54.7	4.6	61.5	29.2	59.6	25.5	54.7	11.2	36.3	30.8
SqueezeSegV2	82.7	21.0	22.6	14.5	15.9	20.2	24.3	2.9	88.5	42.4	65.5	18.7	73.8	41.0	68.5	36.9	58.9	12.9	41.0	39.6
RangeNet++	91.4	25.7	34.4	25.7	23.0	38.3	38.8	4.8	**91.8**	**65.0**	75.2	27.8	87.4	58.6	80.5	55.1	64.6	47.9	55.9	52.5
SalsaNext	**93.2**	51.9	39.3	31.7	**29.3**	60.3	57.8	8.9	91.7	61.3	**75.7**	**29.0**	**89.1**	**61.8**	**83.2**	**64.1**	**67.6**	**53.8**	61.4	58.5
1D-SalsaSAN	**93.2**	**52.2**	**39.8**	**41.4**	28.8	**62.1**	**63.6**	**23.3**	91.2	60.0	75.1	28.5	88.1	60.0	80.8	63.6	64.6	52.9	**63.1**	**59.6**

the 19 classes improved. The IoU of small objects, such as bicycle, motorcycle, person, bicyclist, motorcyclist, and traffic-sign, improved. The IoU of motorcyclist showed the greatest improvement in accuracy with 14.4 pt. This indicates that the 1D-SAB is able to obtain detailed features from the relationships among point clouds and weight objects with a small number of point clouds. Therefore, we can confirm that 1D-SalsaSAN contributes to improving the identification accuracy of small objects. The mIoU is considered to have improved because there are many classes for which 1D-SalsaSAN is highly effective.

textbfComparison of accuracy with conventional methods. From Table 1, 1D-SalsaSAN had the highest mIoU. When the accuracy of each class was compared, the IoU of 8 among the 19 classes was the highest. In particular, the IoU of small objects, the identification accuracy of which was expected to improve, greatly improved. We can also confirm that the accuracy of the remaining classes was almost equal to that of the conventional method with the highest IoU. Therefore, we can say that 1D-SalsaSAN is effective for semantic segmentation.

4.4 Qualitative Results

Figure 4 shows an example of segmentation results using SalsaNext and 1D-SalsaSAN. Our 1D-SalsaSAN was able to identify the correct answer more accurately than SalsaNext. The white boxes in the figure show examples of correct answer and identification results for the traffic-sign class. SalsaNext misidentified part of a traffic-sign as a fence. However, 1D-SalsaSAN was able to correctly identify traffic signs. This qualitatively indicates the effectiveness of 1D-SalsaSAN.

4.5 Comparison of Processing Speed

Figure 5 shows a graph of the relationship between accuracy and processing speed for each method. All processing-speed measurements were conducted using an NVIDIA Quadro RTX A6000. The processing speed of 1D-SalsaSAN was 77.6 Hz, which is 18.0 Hz faster than SalsaNext. We speculate that this is because the computational process of the 1D-SAB is less than that of the context module removed from SalsaNext. The real-time performance of 1D-SalsaSAN is sufficient because omnidirectional LiDAR usually acquires data while rotating at 5 Hz to 20 Hz. SqueezeSeg, which had the fastest processing speed, had the lowest mIoU, as shown in Table 1. SqueezeSegV2 was also faster than 1D-SalsaSAN, but its mIoU was 20.0 ppt lower than 1D-SalsaSAN. For autonomous driving tasks, both accuracy and speed are important metrics, so 1D-SalsaSAN is the most effective for semantic segmentation in terms of both.

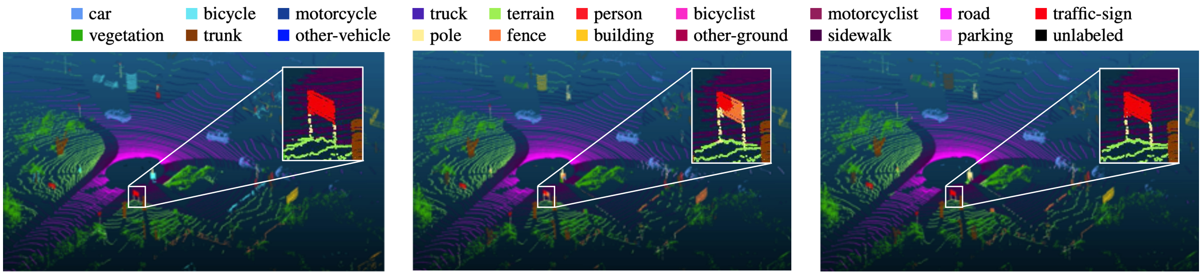

(a) Ground truth (b) SalsaNext (c) 1D-SalsaSAN

Figure 4: Examples of segmentation results.

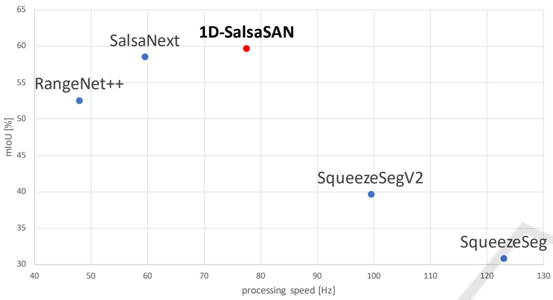

Figure 5: Relationship between accuracy and processing speed for each method.

5 CONCLUSIONS

We proposed 1D-SalsaSAN, which uses a 1D-SAB to improve the identification accuracy for small objects. From the evaluation experiments, we confirmed that the 1D-SAB improves the overall segmentation accuracy, especially for small objects. The processing speed also improved compared which that of SalsaNext, indicating that the real-time performance required for autonomous driving was sufficiently maintained. Our future work includes further improvement in identification accuracy through data augmentation, confirmation of the generalizability of 1D-SalsaSAN through evaluation experiments using other data sets, and investigation of the network structure.

REFERENCES

Aksoy, E. E., Baci, S., and Cavdar, S. (2020). Salsanet: Fast road and vehicle segmentation in lidar point clouds for autonomous driving. In *2020 IEEE Intelligent Vehicles Symposium (IV)*, pages 926–932.

Alonso, I., Riazuelo, L., Montesano, L., and Murillo, A. C. (2020). 3d-mininet: Learning a 2d representation from point clouds for fast and efficient 3d lidar semantic segmentation. *IEEE Robotics and Automation Letters*, 5(4):5432–5439.

Behley, J., Garbade, M., Milioto, A., Quenzel, J., Behnke, S., Stachniss, C., and Gall, J. (2019). SemanticKITTI: A Dataset for Semantic Scene Understanding of LiDAR Sequences. In *Proc. of the IEEE/CVF International Conf. on Computer Vision (ICCV)*.

Berman, M., Rannen Triki, A., and Blaschko, M. B. (2018). The lovász-softmax loss: A tractable surrogate for the optimization of the intersection-over-union measure in neural networks. In *Proceedings of the IEEE Conference on Computer Vision and Pattern Recognition*, pages 4413–4421.

Cheng, R., Razani, R., Taghavi, E., Li, E., and Liu, B. (2021). (af)2-s3net: Attentive feature fusion with adaptive feature selection for sparse semantic segmentation network. In *Proceedings of the IEEE/CVF Conference on Computer Vision and Pattern Recognition (CVPR)*, pages 12547–12556.

Cortinhal, T., Tzelepis, G., and Aksoy, E. E. (2020). Salsanext: Fast, uncertainty-aware semantic segmentation of lidar point clouds for autonomous driving.

Ding, L. and Feng, C. (2019). Deepmapping: Unsupervised map estimation from multiple point clouds. In *Proceedings of the IEEE/CVF Conference on Computer Vision and Pattern Recognition (CVPR)*.

Geiger, A., Lenz, P., and Urtasun, R. (2012). Are we ready for Autonomous Driving? The KITTI Vision Benchmark Suite. In *Proc. of the IEEE Conf. on Computer Vision and Pattern Recognition (CVPR)*, pages 3354–3361.

He, K., Zhang, X., Ren, S., and Sun, J. (2016). Deep residual learning for image recognition. In *Proceedings of the IEEE Conference on Computer Vision and Pattern Recognition (CVPR)*.

Lin, D., Ji, Y., Lischinski, D., Cohen-Or, D., and Huang, H. (2018). Multi-scale context intertwining for semantic segmentation. In *Proceedings of the European Conference on Computer Vision (ECCV)*.

Liu, X., Qi, C. R., and Guibas, L. J. (2019). Flownet3d: Learning scene flow in 3d point clouds. In *Proceedings of the IEEE/CVF Conference on Computer Vision and Pattern Recognition (CVPR)*.

Maturana, D. and Scherer, S. (2015). Voxnet: A 3d convolutional neural network for real-time object recognition. In *2015 IEEE/RSJ International Conference on Intelligent Robots and Systems (IROS)*, pages 922–928.

Meyer, G. P., Laddha, A., Kee, E., Vallespi-Gonzalez, C., and Wellington, C. K. (2019). Lasernet: An efficient probabilistic 3d object detector for autonomous driving. In *Proceedings of the IEEE/CVF Conference on Computer Vision and Pattern Recognition (CVPR)*.

Milioto, A., Vizzo, I., Behley, J., and Stachniss, C. (2019). Rangenet ++: Fast and accurate lidar semantic segmentation. In *2019 IEEE/RSJ International Conference on Intelligent Robots and Systems (IROS)*, pages 4213–4220.

Qi, C. R., Su, H., Kaichun, M., and Guibas, L. J. (2017a). Pointnet: Deep learning on point sets for 3d classification and segmentation. In *IEEE Conference on Computer Vision and Pattern Recognition*, pages 77–85.

Qi, C. R., Yi, L., Su, H., and Guibas, L. J. (2017b). Pointnet++: Deep hierarchical feature learning on point sets in a metric space. *arXiv preprint arXiv:1706.02413*.

Rosu, R. A., Schütt, P., Quenzel, J., and Behnke, S. (2019). Latticenet: Fast point cloud segmentation using permutohedral lattices. *CoRR*, abs/1912.05905.

Shi, S., Guo, C., Jiang, L., Wang, Z., Shi, J., Wang, X., and Li, H. (2020). Pv-rcnn: Point-voxel feature set abstraction for 3d object detection. In *Proceedings of the IEEE/CVF Conference on Computer Vision and Pattern Recognition (CVPR)*.

Shi, W., Caballero, J., Huszar, F., Totz, J., Aitken, A. P., Bishop, R., Rueckert, D., and Wang, Z. (2016). Real-time single image and video super-resolution using an efficient sub-pixel convolutional neural network. In *Proceedings of the IEEE Conference on Computer Vision and Pattern Recognition (CVPR)*.

Simony, M., Milzy, S., Amendey, K., and Gross, H.-M. (2018). Complex-yolo: An euler-region-proposal for real-time 3d object detection on point clouds. In *Proceedings of the European Conference on Computer Vision (ECCV) Workshops*.

Triess, L. T., Peter, D., Rist, C. B., and Zollner, J. M. (2020). Scan-based semantic segmentation of lidar point clouds: An experimental study. In *2020 IEEE Intelligent Vehicles Symposium (IV)*, pages 1116–1121.

Wu, B., Wan, A., Yue, X., and Keutzer, K. (2018). Squeezeseg: Convolutional neural nets with recurrent crf for real-time road-object segmentation from 3d lidar point cloud. *ICRA*.

Wu, B., Zhou, X., Zhao, S., Yue, X., and Keutzer, K. (2019). Squeezesegv2: Improved model structure and unsupervised domain adaptation for road-object segmentation from a lidar point cloud. In *ICRA*.

Zhao, H., Jia, J., and Koltun, V. (2020). Exploring self-attention for image recognition. In *CVPR*.

Zhou, Y. and Tuzel, O. (2018). Voxelnet: End-to-end learning for point cloud based 3d object detection. In *IEEE Conference on Computer Vision and Pattern Recognition*, pages 4490–4499.